Electronic Supplementary Information

Title: Enhancing adsorption-photocatalytic efficiency of BiOBr for Congo red degradation by tuning surface charge and bandgap *via* Y^{3+}-I^- co-doping strategy

Authors and affiliations:

Dongsheng Chen [a], Keqian Gong [b], Xiangyang Xu [a, c, *], Chenyu Huang [a], Pengtao Lei [a]

a School of Minerals Processing and Bioengineering, Central South University, Changsha 410083, China

b. State Key Laboratory of New Ceramics and Fine Processing, Institute of Nuclear and New Energy Technology, Tsinghua University, Beijing, 100084, China

c Hunan Key Laboratory of Mineral Materials and Applications, Changsha 410083, China

Corresponding author: Xiangyang Xu (E-mail: xuxiangyang@csu.edu.cn)

This *Supplementary Material* file contains 12 figures showing SEM, XRD, TEM, FTIR, Adsorption-photodegradation and calculation results. Meanwhile, 11 relevant data tables were supplied.

Figure captions:

Fig. S1. Wide-field SEM images of BiOBr (a), $Bi_{0.8}Y_{0.20}OBr$ (b), $BiOBr_{0.97}I_{0.03}$ (c) and $Bi_{0.8}Y_{0.20}OBr_{0.97}I_{0.03}$ (d).

Fig. S2. XRD patterns of $Bi_{1-x}Y_xOBr$ (a), $BiOBr_{1-y}I_y$ (b) and $Bi_{0.8}Y_{0.2}OBr_{1-y}I_y$ (c).

Fig. S3. TEM visualization (top side view on flake surface) of pristine BiOBr (a) and $Bi_{0.8}Y_{0.2}OBr_{0.97}I_{0.03}$ (b).

Fig. S4. SAED patterns of pristine BiOBr (a) and $Bi_{0.8}Y_{0.2}OBr_{0.97}I_{0.03}$ (b).

Fig. S5. HRTEM visualization (sectional profile) of pristine BiOBr (a) and $Bi_{0.8}Y_{0.2}OBr_{0.97}I_{0.03}$ (b).

Fig. S6. HRTEM and localized magnified fast Fourier transform images of pristine BiOBr (a, a1 and a2) showing orderly array and $Bi_{0.8}Y_{0.2}OBr_{0.97}I_{0.03}$ (b, b1 and b2) displaying a defect-rich structure.

Fig. S7. COHP images of $Bi_{0.8}Y_{0.2}OBr$ (a), $BiOBr_{0.97}I_{0.03}$ (b) and $Bi_{0.8}Y_{0.2}OBr_{0.97}I_{0.03}$ (c). The interactions between those atoms are described by the product of their corresponding Hamiltonian matrix element and the density of states matrix.

Fig. S8. FTIR spectra for bands over 4000-2700 cm^{-1}(a) and 1800-400 cm^{-1} (b) of BiOBr, $Bi_{0.8}Y_{0.2}OBr$, $BiOBr_{0.97}I_{0.03}$, $Bi_{0.8}Y_{0.2}OBr_{0.97}I_{0.03}$ and PVP K30.

Fig. S9. FTIR spectra of CR.

Fig. S10. Adsorption-photodegradation curves and pseudo-first-order kinetic plots of $Bi_{0.8}Y_{0.2}OBr_{1-y}I_y$ (initial CR solution: 100 mL, pH: 6, and catalyst dosage: 25 mg).

Fig. S11. Cycling performance of CR photodegradation for $Bi_{0.8}Y_{0.2}OBr_{0.97}I_{0.03}$.

Fig. S12. XRD patterns of the fresh and cycled $Bi_{0.8}Y_{0.2}OBr_{0.97}I_{0.03}$.

Table captions:

Table S1. BET special surface area, pore volume and modal pore size of pure BiOBr, $Bi_{0.8}Y_{0.2}OBr$, $BiOBr_{0.97}I_{0.03}$ and $Bi_{0.8}Y_{0.2}OBr_{0.97}I_{0.03}$.

Table S2. Lattice constants of pristine and doped BiOBr samples based on Rietveld method.

Table S3 Bond length of pristine and doped BiOBr structures.

Table S4 Lattice constant and angle of pristine and doped BiOBr structures.

Table S5. Assignment of main FTIR peaks of PVP K30, pristine and doped BiOBr powders.

Table S6. Assignment of main FTIR peaks of CR.

Table S7. Calculated E_{fb}, E_{CB} and E_{VB} values of BiOBr samples using Mott-Schottky equation.

Table S8. DFT calculated band structural results of pure and doped BiOBr flakes.

Table S9. Adsorption efficiency, photodegradation efficiency, first-order kinetic parameters for different samples (initial CR concentration: 50 mg L^{-1}, CR solution: 50 mL, pH: 6, and catalyst dosage: 25 mg).

Table S10. TOC removal performance of $Bi_{0.8}Y_{0.2}OBr_{0.97}I_{0.03}$ for the degradation of CR.

Table S11. Adsorption efficiency, photodegradation efficiency, first-order kinetic parameters for different samples (initial CR concentration: 100 mg L^{-1}, CR solution: 50 mL, pH: 6, and catalyst dosage: 25 mg).

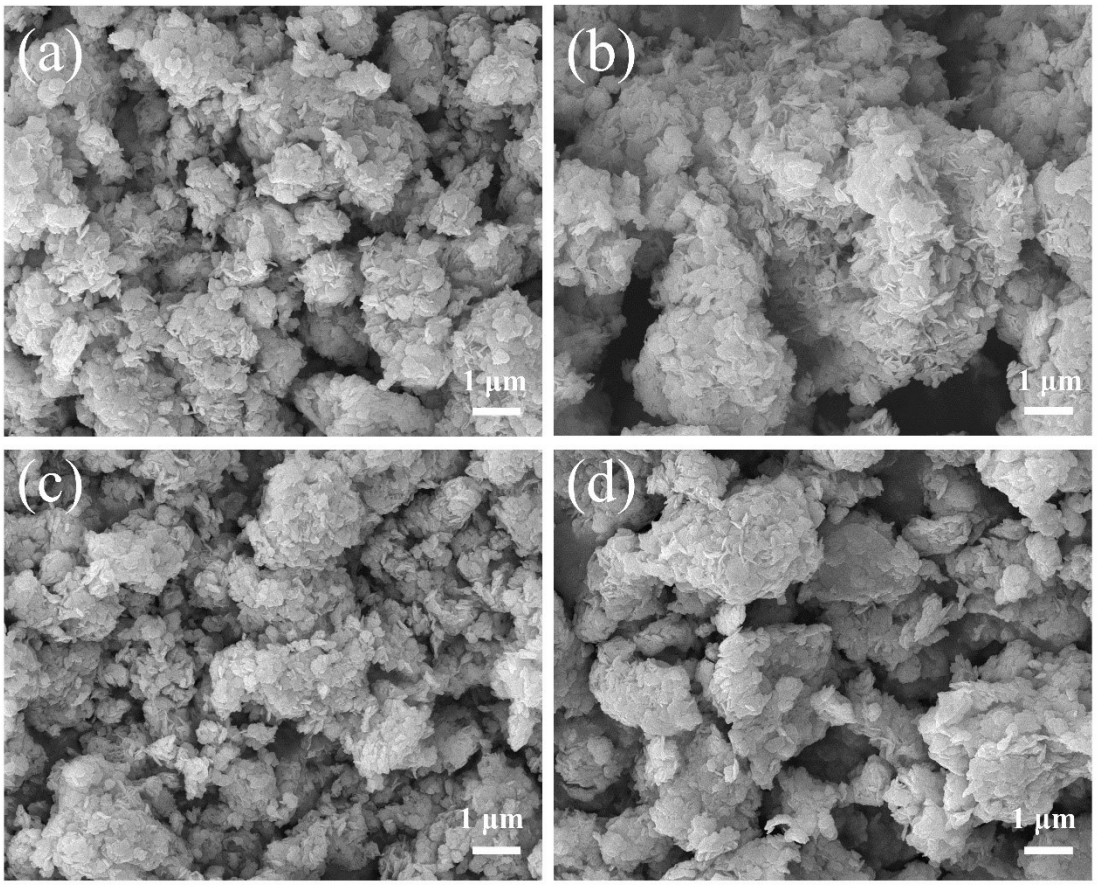

Fig. S1. Wide-field SEM images of BiOBr (a), $Bi_{0.8}Y_{0.2}OBr$ (b), $BiOBr_{0.97}I_{0.03}$ (c) and $Bi_{0.8}Y_{0.2}OBr_{0.97}I_{0.03}$ (d).

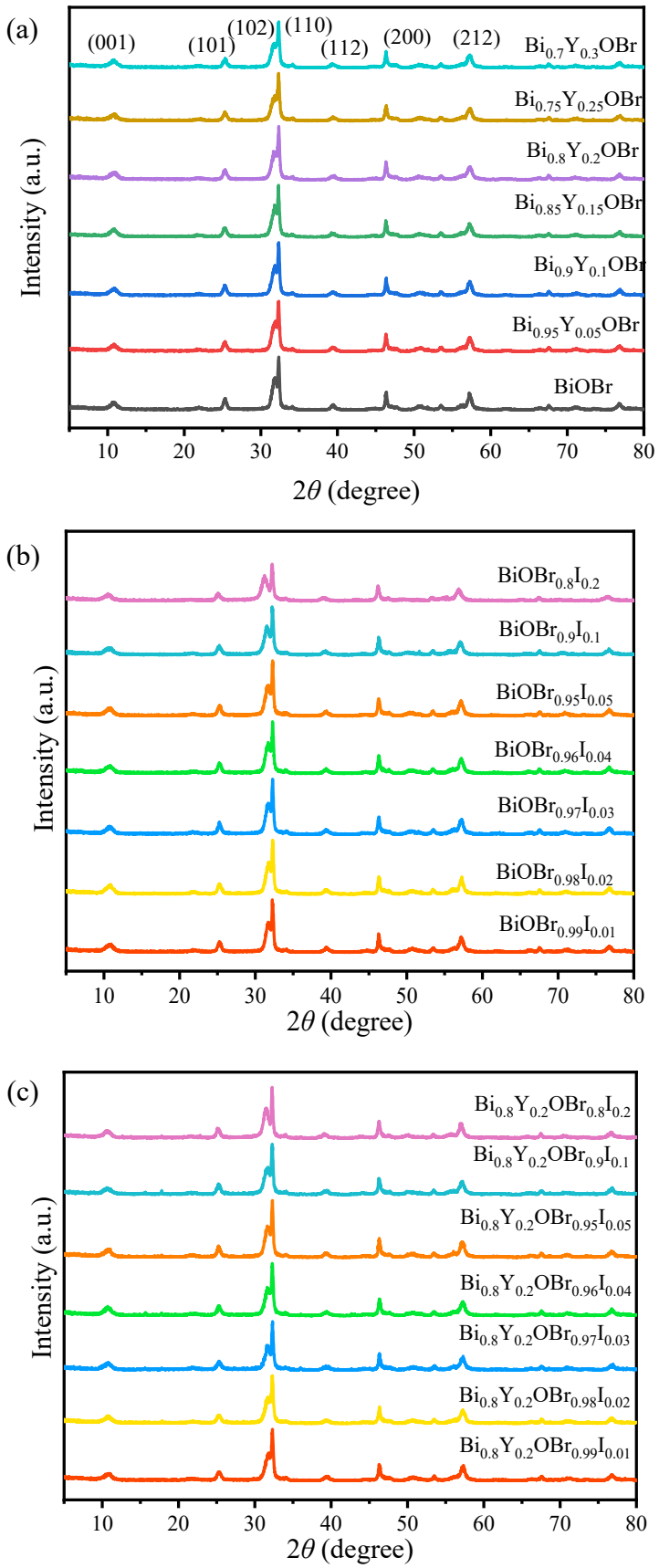

Fig. S2. XRD patterns of $Bi_{1-x}Y_xOBr$ (a), $BiOBr_{1-y}I_y$ (b) and $Bi_{0.8}Y_{0.2}OBr_{1-y}I_y$ (c).

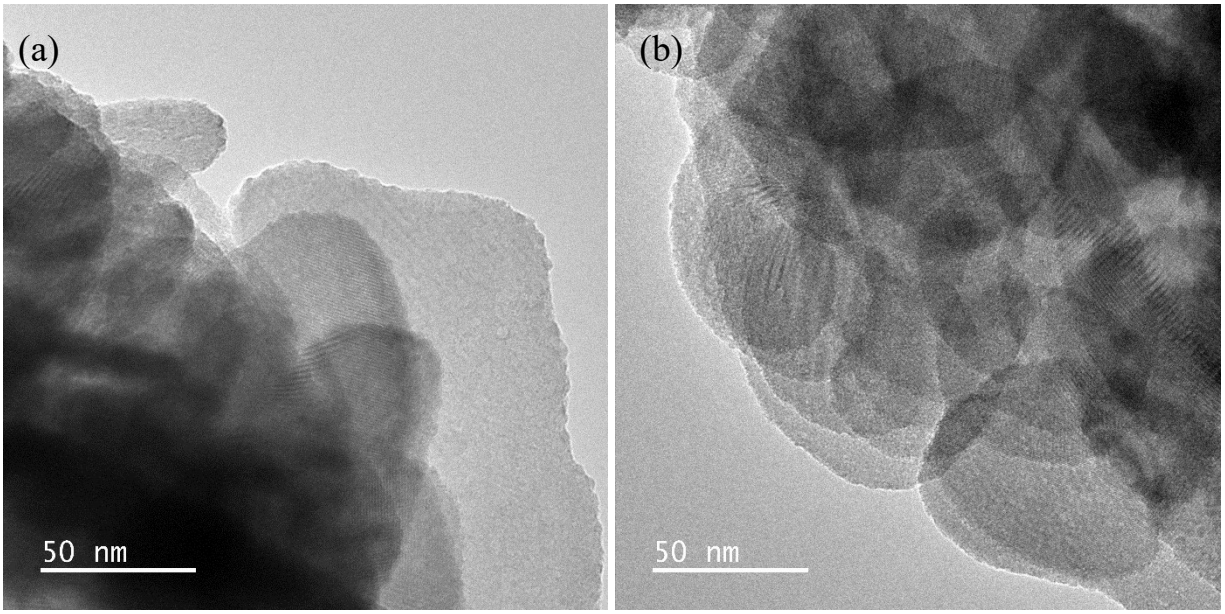

Fig. S3. TEM visualization (top side view on flake surface) of pristine BiOBr (a) and $Bi_{0.8}Y_{0.2}OBr_{0.97}I_{0.03}$ (b).

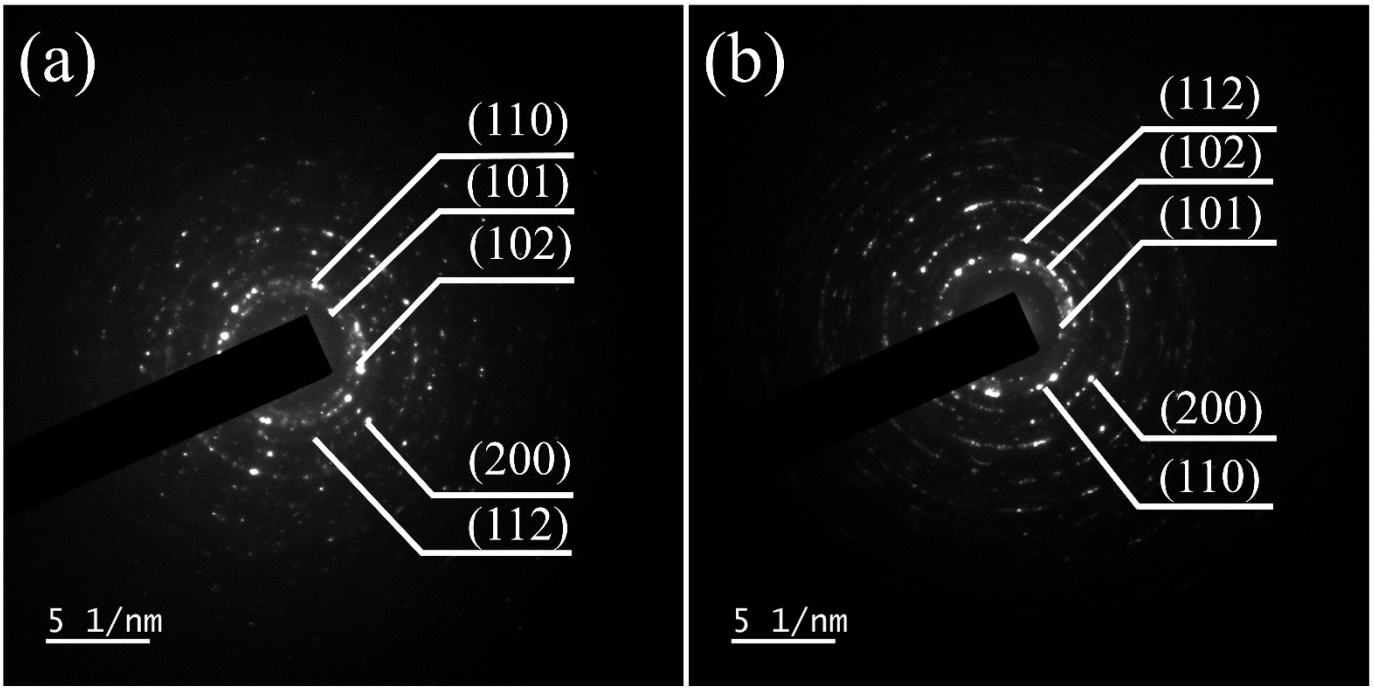

Fig. S4. SAED patterns of pristine BiOBr (a) and $Bi_{0.8}Y_{0.2}OBr_{0.97}I_{0.03}$ (b).

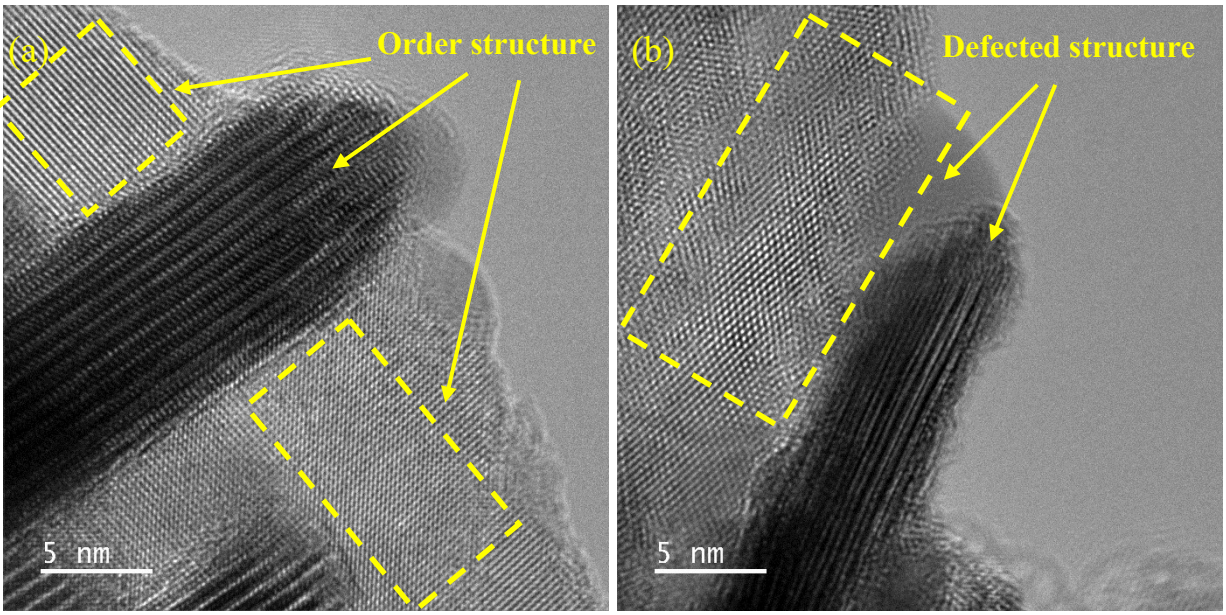

Fig. S5. HRTEM visualization (sectional profile) of pristine BiOBr (a) and $Bi_{0.8}Y_{0.2}OBr_{0.97}I_{0.03}$ (b).

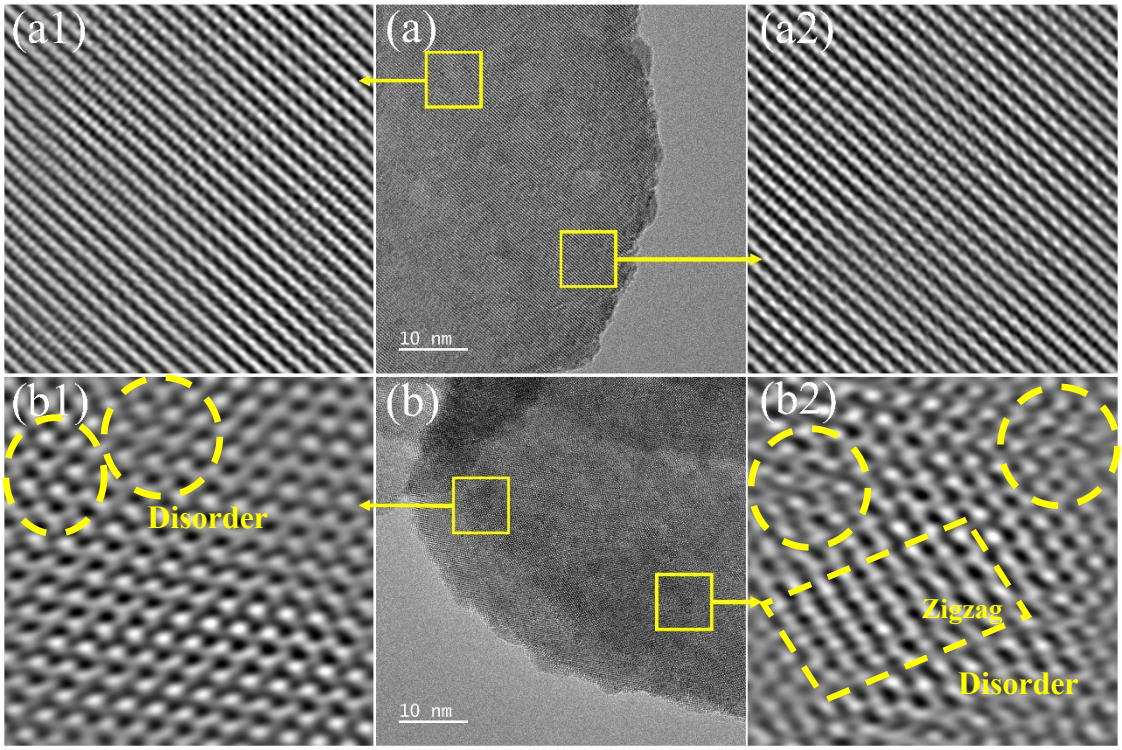

Fig. S6. HRTEM and localized magnified fast Fourier transform images of pristine BiOBr (a, a1 and a2) showing orderly array and $Bi_{0.8}Y_{0.2}OBr_{0.97}I_{0.03}$ (b, b1 and b2) displaying a defect-rich structure.

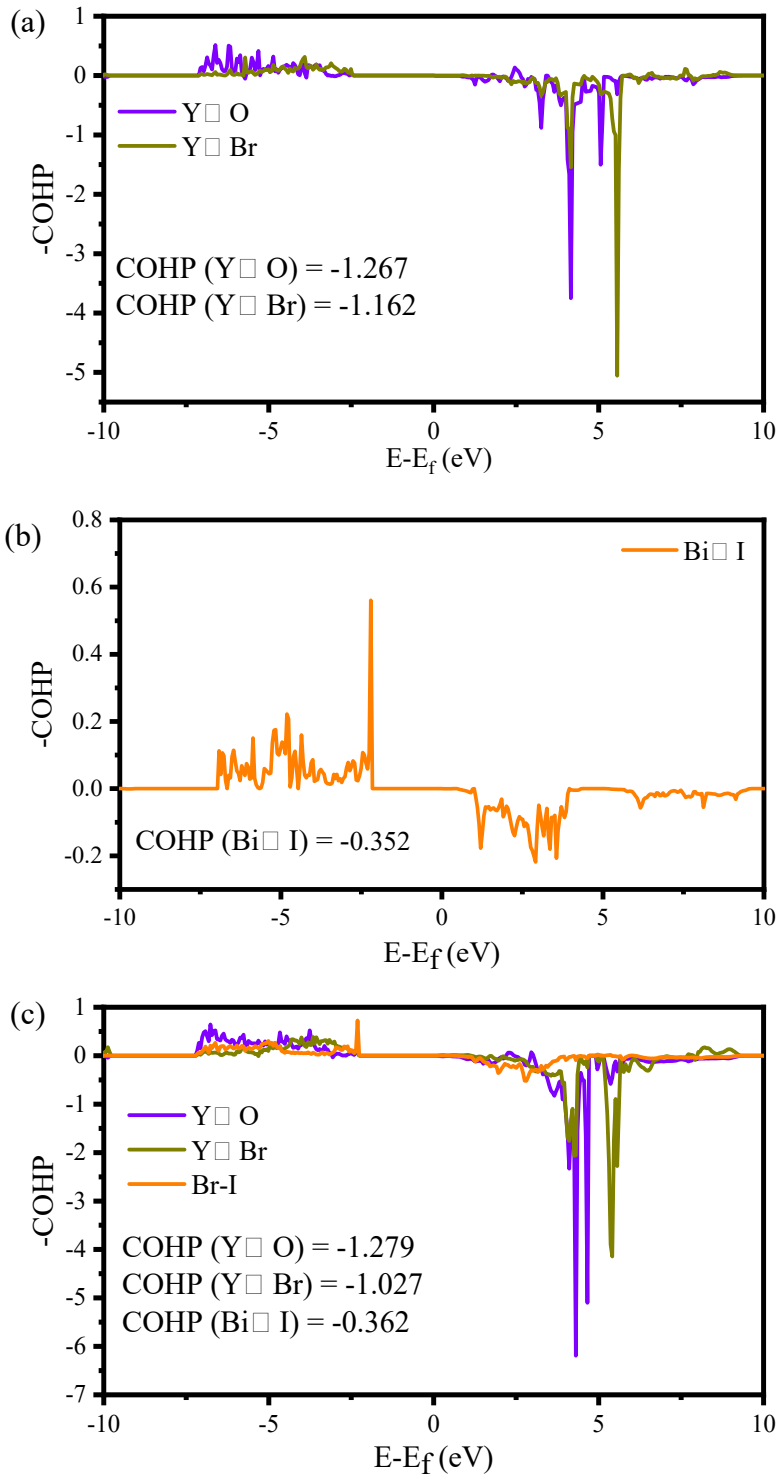

Fig. S7. COHP images of $Bi_{0.8}Y_{0.2}OBr$ (a), $BiOBr_{0.97}I_{0.03}$ (b) and $Bi_{0.8}Y_{0.2}OBr_{0.97}I_{0.03}$ (c). The interactions between those atoms are described by the product of their corresponding Hamiltonian matrix element and the density of states matrix.

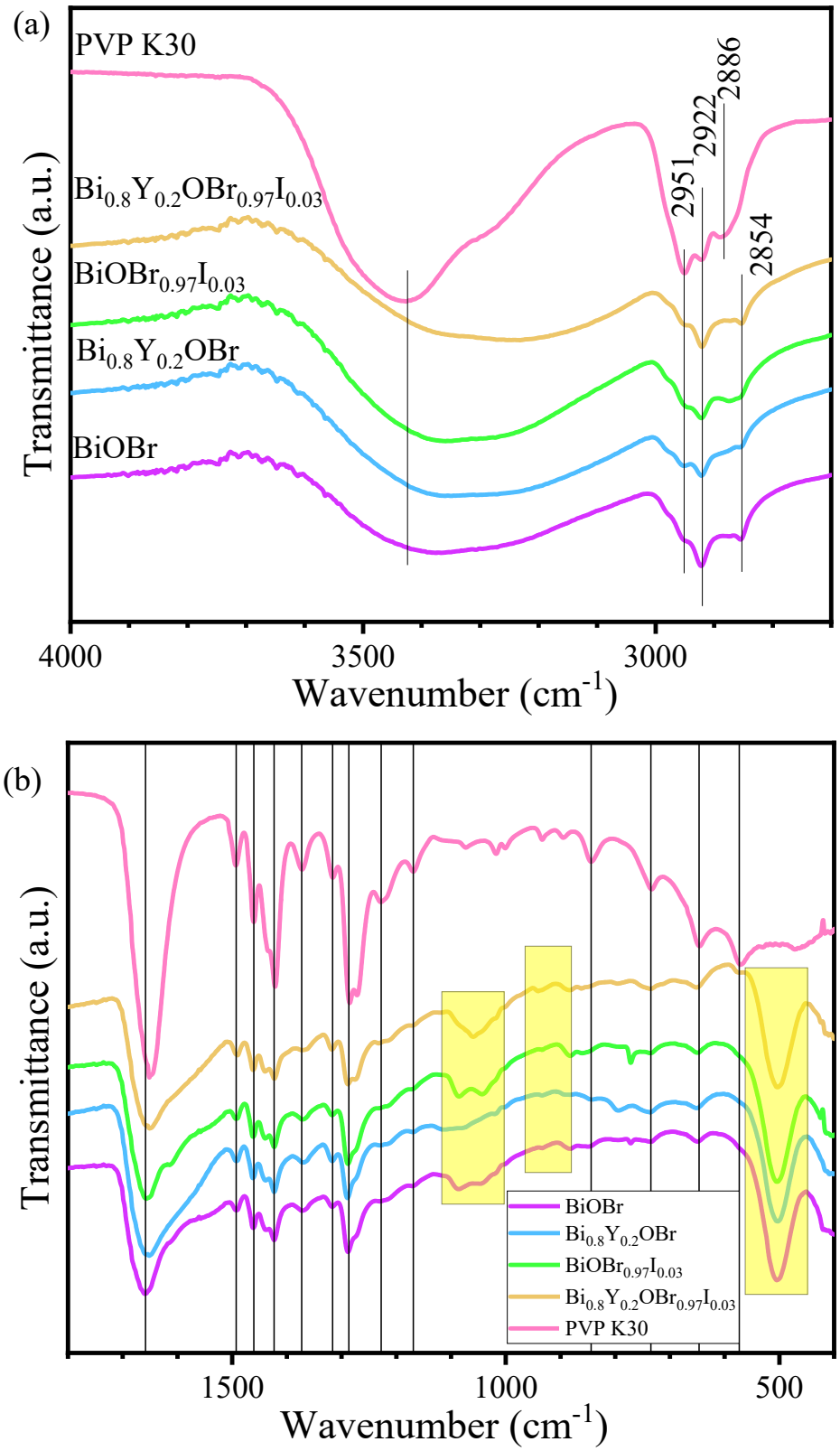

Fig. S8. FTIR spectra for bands over 4000-2700 cm^{-1}(a) and 1800-400 cm^{-1} (b) of BiOBr, $Bi_{0.8}Y_{0.2}OBr$, $BiOBr_{0.97}I_{0.03}$, $Bi_{0.8}Y_{0.2}OBr_{0.97}I_{0.03}$ and PVP K30.

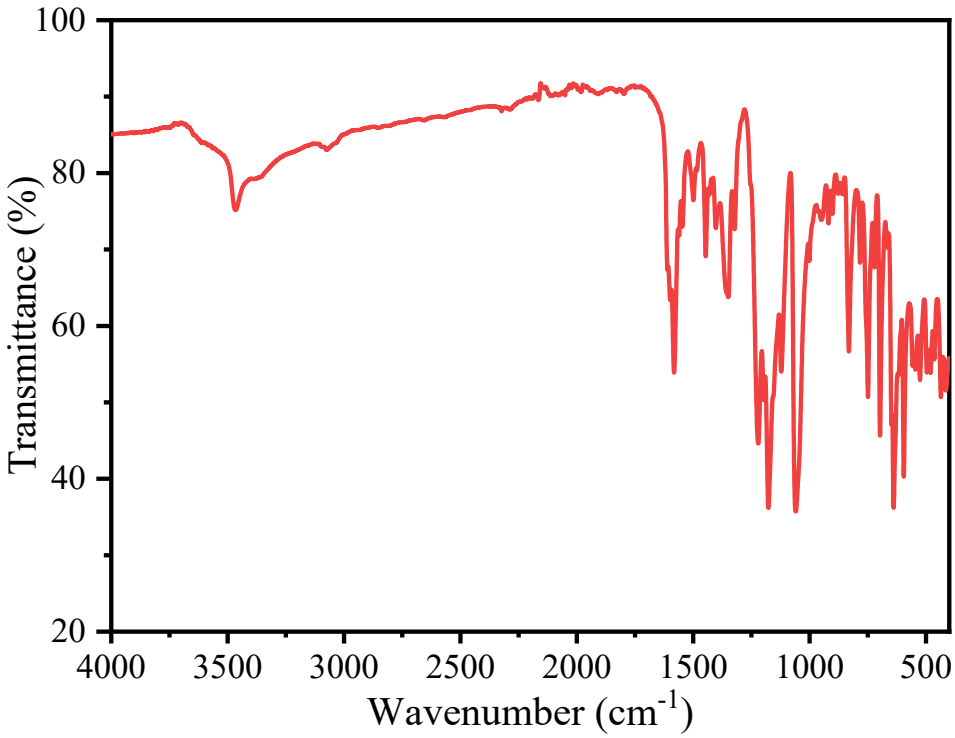

Fig. S9. FTIR spectra of CR.

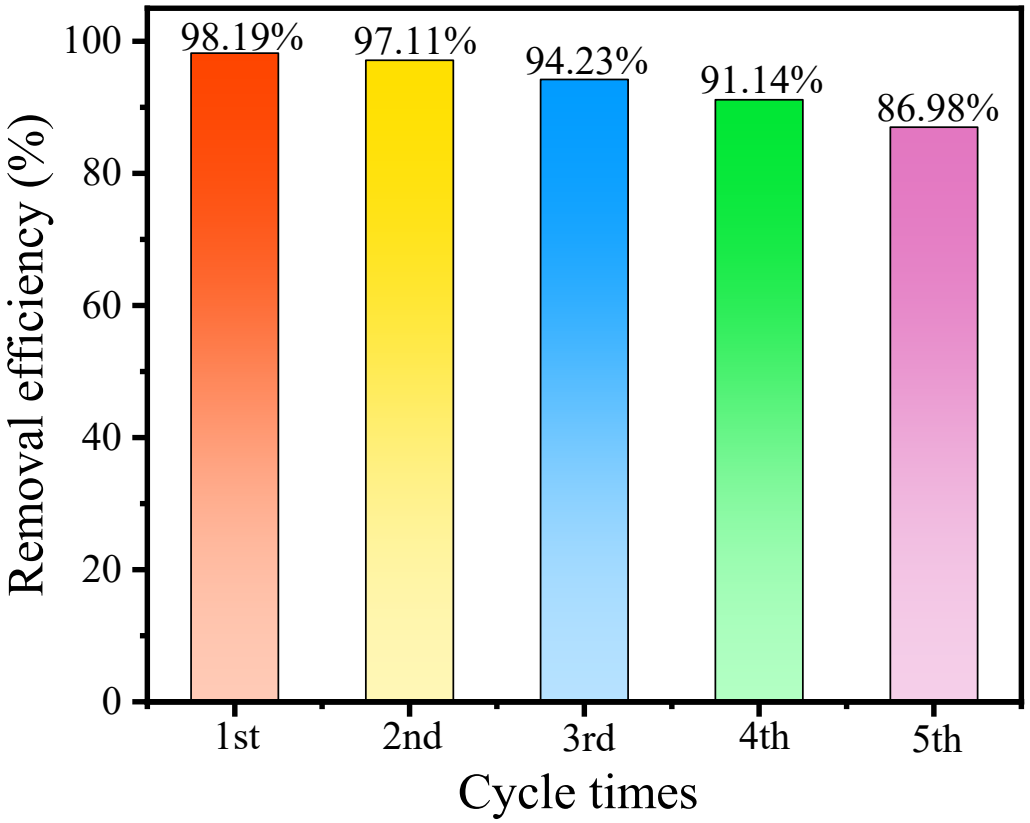

Fig. S10. Cycling performance of CR photodegradation for $Bi_{0.8}Y_{0.2}OBr_{0.97}I_{0.03}$.

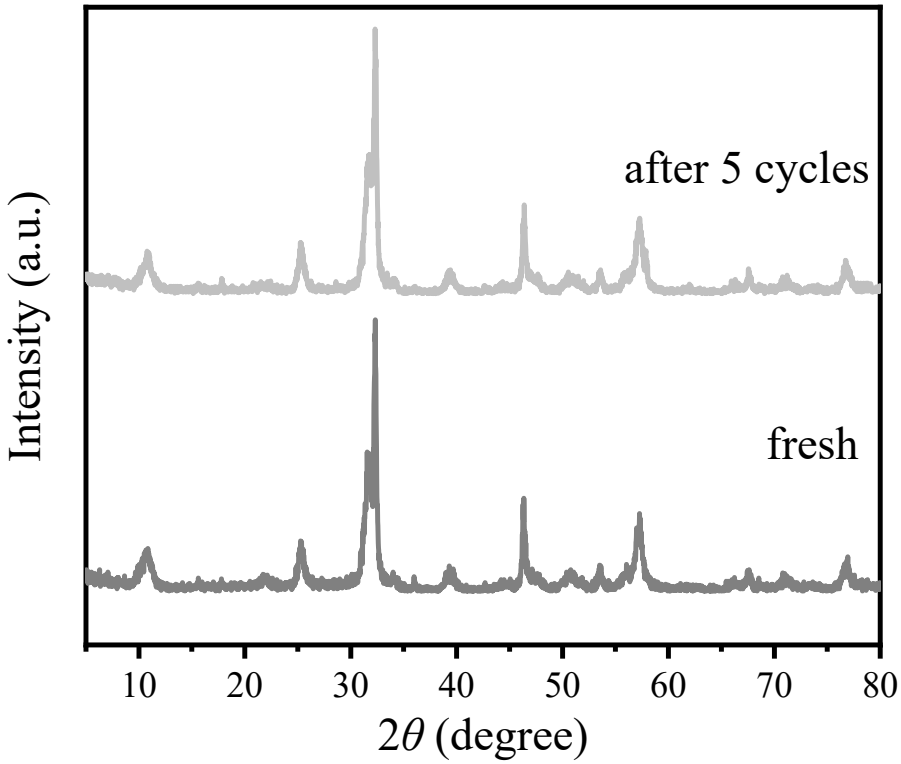

Fig. S11. XRD patterns of the fresh and cycled $Bi_{0.8}Y_{0.2}OBr_{0.97}I_{0.03}$.

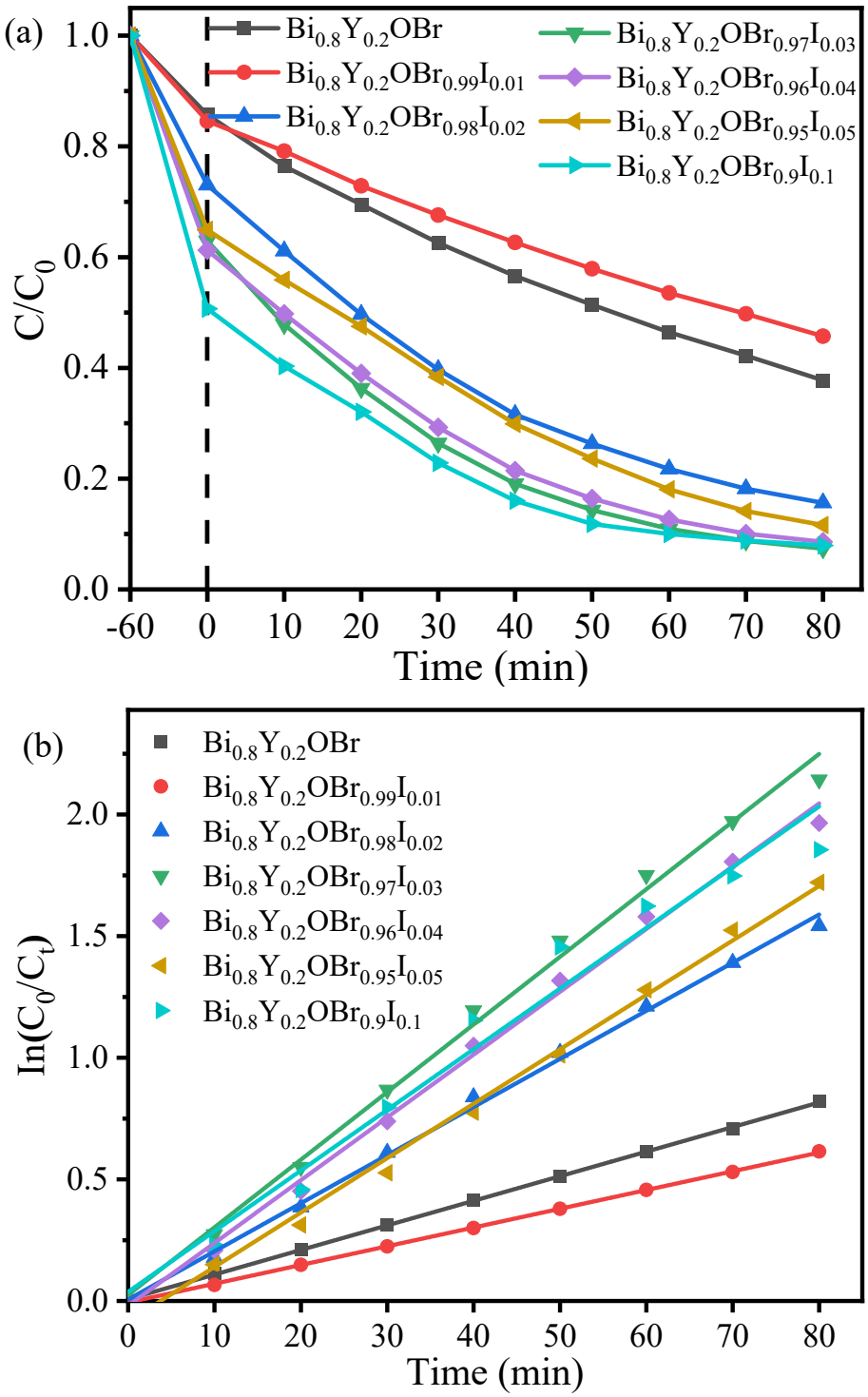

Fig. S12. Adsorption-photodegradation curves and pseudo-first-order kinetic plots of $Bi_{0.8}Y_{0.2}OBr_{1-y}I_y$ (initial CR concentration: 100 mg L^{-1}, solution volume: 50 mL, pH: 6, and catalyst dosage: 25 mg).

Table S1 BET special surface area, pore volume and modal pore size of pure BiOBr, $Bi_{0.8}Y_{0.2}OBr$, $BiOBr_{0.97}I_{0.03}$ and $Bi_{0.8}Y_{0.2}OBr_{0.97}I_{0.03}$.

Samples	S_{BET} (m^2 g^{-1})	Pore volume (cm^3 g^{-1})	Modal pore diameter (nm)
BiOBr	32.7069	0.242811	29.6954
$Bi_{0.8}Y_{0.2}OBr$	33.5234	0.265345	30.5459
$BiOBr_{0.97}I_{0.03}$	33.9161	0.228927	25.9945
$Bi_{0.8}Y_{0.2}OBr_{0.97}I_{0.03}$	30.0059	0.196479	26.1920

Table S2 Lattice constants of pristine and doped BiOBr samples based on Rietveld method.

Lattice constant (Å)	*a=b*	*c*
BiOBr	3.91985	8.09339
$Bi_{0.95}Y_{0.05}OBr$	3.92506	8.11091
$Bi_{0.9}Y_{0.1}OBr$	3.92444	8.1064
$Bi_{0.85}Y_{0.15}OBr$	3.92369	8.0982
$Bi_{0.8}Y_{0.2}OBr$	3.92282	8.09552
$Bi_{0.75}Y_{0.25}OBr$	3.92187	8.09011
$Bi_{0.7}Y_{0.3}OBr$	3.92095	8.08639
$BiOBr_{0.99}I_{0.01}$	3.92052	8.12369
$BiOBr_{0.98}I_{0.02}$	3.92387	8.12452
$BiOBr_{0.97}I_{0.03}$	3.92429	8.1267
$BiOBr_{0.96}I_{0.04}$	3.9257	8.1311
$BiOBr_{0.95}I_{0.05}$	3.92765	8.13359
$BiOBr_{0.9}I_{0.1}$	3.92836	8.20445
$BiOBr_{0.8}I_{0.2}$	3.92909	8.41192
$Bi_{0.8}Y_{0.2}OBr_{0.99}I_{0.01}$	3.927	8.1151
$Bi_{0.8}Y_{0.2}OBr_{0.98}I_{0.02}$	3.92911	8.12311
$Bi_{0.8}Y_{0.2}OBr_{0.97}I_{0.03}$	3.93012	8.12843
$Bi_{0.8}Y_{0.2}OBr_{0.96}I_{0.04}$	3.93249	8.13555
$Bi_{0.8}Y_{0.2}OBr_{0.95}I_{0.05}$	3.93402	8.14834
$Bi_{0.8}Y_{0.2}OBr_{0.9}I_{0.1}$	3.93255	8.19480
$Bi_{0.8}Y_{0.2}OBr_{0.8}I_{0.2}$	3.92753	8.23199

Table S3 Bond length of pristine and doped BiOBr structures.

Sample	Bond length (Å)				
	Bi−O	Bi−Br	Y−O	Y−Br	Bi−I
BiOBr	2.347	3.220	/	/	/
$Bi_{0.8}Y_{0.2}OBr$	2.316	3.306	2.291	3.118	/
$BiOBr_{0.97}I_{0.03}$	2.344	3.241	/	/	3.380
$Bi_{0.8}Y_{0.2}OBr_{0.97}I_{0.03}$	2.342	3.255	2.305	3.092	3.369

Table S4 Lattice constant and angle of pristine and doped BiOBr structures.

Sample	Lattice constant (Å)			Angle (°)		
	a	*b*	*c*	*α*	*β*	*γ*
BiOBr	7.89672	7.89672	9.05605	90.00	90.00	90.00
$Bi_{0.8}Y_{0.2}OBr$	7.89788	7.86302	8.90773	90.00	90.00	90.00
$BiOBr_{0.97}I_{0.03}$	7.90587	7.90375	8.96267	90.00	90.00	90.00
$Bi_{0.8}Y_{0.2}OBr_{0.97}I_{0.03}$	7.88784	7.88619	8.96776	90.02	89.99	90.01

Table S5 Assignment of main FTIR peaks of PVP K30, pristine and doped BiOBr powders.

Peak center /cm^{-1}	Absorption mode				
	PVP	Raw BiOBr	$Bi_{0.8}Y_{0.2}OBr$	$BiOBr_{0.97}I_{0.03}$	$Bi_{0.8}Y_{0.2}OBr_{0.97}I_{0.03}$
3700-3000		C═O, Overtone； ν_{O-H}			
3427	C═O, Overtone				
2951	$\nu_{as\ -CH_2}$	$\nu_{as\ -CH_2}$			
2922	$\nu_{s\ -CH_2}$	$\nu_{s\ -CH_2}$			
2886	ν_{-CH}				
2854		ν_{-CH}			
1652	$\nu_{C=O}$, ν_{C-N}				
1658-1650		$\nu_{C=O}$, ν_{C-N}, δ_{H-O-H}			
1494	ν_{C-N}	ν_{C-N}			
1461	δ_{-CH_2}	δ_{-CH_2}			
1422	δ_{-CH_2}	δ_{-CH_2}			
1372	γ_{-CH}	γ_{-CH}			
1317	ω_{-CH_2} . ν_{C-N}	ω_{-CH_2} . ν_{C-N}			
1280					
1238					
1169	τ_{-CH_2}				
1087		Bi-OH			
1060					-O-H···O=C
1041		-O-H···O=C			
1018	ρ_{-CH2}				
884		Bi-O			
845	C−C, ring				
733	C−C, chain	C−C, chain			
647	$\delta_{N-C=O}$	$\delta_{N-C=O}$			
506		Bi-O			

Table S6 Assignment of main FTIR peaks of CR.

Peak center /cm^{-1}	Absorption mode
3466	N–H stretching
3076	C–H stretching
1582	–N=N– stretching
1499	C–C stretching
1446	C=C stretching, aromatic
1349	C–N bending
1223, 1176, 1057	C-N stretching (Alkyl), $-SO_3^-$ stretching, CH in-plane deformation
832	C−C, ring
749	CH wagging, ring deformation
695, 661, 597	$-SO_3^-$ bending, N-H out-of-plane deformation, C-H (ring) wagging
646	C–C twisting

Table S7 Calculated E_{fb}, E_{CB} and E_{VB} values of BiOBr samples using Mott-Schottky equation.

Samples	E_g (eV)	*x*-axis intercept	E_{fb} V *vs* Ag/AgCl	E_{CB} (eV)	E_{VB} (eV)
BiOBr	2.73	-0.13	-0.16	0.04	2.77
$Bi_{0.8}Y_{0.2}OBr$	2.78	-0.71	-0.74	-0.54	2.24
$BiOBr_{0.97}I_{0.03}$	2.30	-0.28	-0.31	-0.11	2.19
$Bi_{0.8}Y_{0.2}OBr_{0.97}I_{0.03}$	2.38	-0.55	-0.58	-0.38	2.0

Table S8. DFT calculated band structural results of pure and doped BiOBr flakes.

Sample	DFT			
	Fermi Energy	Band gap	W_{VBM}	W_{CBM}
BiOBr	2.74	2.32	2.30	-0.0163
$Bi_{0.8}Y_{0.2}OBr$	2.75	2.41	2.40	-0.0192
$BiOBr_{0.97}I_{0.03}$	3.005	2.25	2.219	-0.0285
$Bi_{0.8}Y_{0.2}OBr_{0.97}I_{0.03}$	3.712	2.29	2.281	-0.0084

Table S9. Adsorption efficiency, photodegradation efficiency, first-order kinetic parameters for different samples (initial CR concentration: 50 mg L^{-1}, CR solution: 50 mL, pH: 6, and catalyst dosage: 25 mg).

Samples	Adsorption efficiency (%)	Adsorption+ Photodegradation efficiency (%)	k (min^{-1})	R^2
BiOBr	10.60	46.51	0.00637	0.99882
$Bi_{0.95}Y_{0.05}OBr$	20.40	82.55	0.01945	0.99744
$Bi_{0.9}Y_{0.1}OBr$	28.52	86.91	0.02209	0.94075
$Bi_{0.85}Y_{0.15}OBr$	25.64	86.98	0.02246	0.98043
$Bi_{0.8}Y_{0.2}OBr$	31.21	90.87	0.02444	0.91122
$Bi_{0.75}Y_{0.25}OBr$	26.04	86.11	0.02117	0.98468
$Bi_{0.7}Y_{0.3}OBr$	30.40	89.66	0.02374	0.92754
$BiOBr_{0.99}I_{0.01}$	16.91	71.21	0.01329	0.99926
$BiOBr_{0.98}I_{0.02}$	14.56	71.48	0.01373	0.99823
$BiOBr_{0.97}I_{0.03}$	15.17	76.64	0.0162	0.999
$BiOBr_{0.96}I_{0.04}$	14.77	67.72	0.01217	0.99966
$BiOBr_{0.95}I_{0.05}$	14.56	75.44	0.01568	0.99883
$BiOBr_{0.9}I_{0.1}$	16.11	80.00	0.01817	0.99658
$Bi_{0.8}Y_{0.2}OBr_{0.99}I_{0.01}$	28.99	84.77	0.02005	0.99967
$Bi_{0.8}Y_{0.2}OBr_{0.98}I_{0.02}$	57.65	90.47	0.01997	0.99295
$Bi_{0.8}Y_{0.2}OBr_{0.97}I_{0.03}$	75.71	98.19	0.03653	0.98115
$Bi_{0.8}Y_{0.2}OBr_{0.96}I_{0.04}$	75.77	97.85	0.03497	0.99499
$Bi_{0.8}Y_{0.2}OBr_{0.95}I_{0.05}$	65.44	97.11	0.03629	0.99603
$Bi_{0.8}Y_{0.2}OBr_{0.9}I_{0.1}$	82.01	97.85	0.03019	0.97519

Table S10. TOC removal performance of $Bi_{0.8}Y_{0.2}OBr_{0.97}I_{0.03}$ for the degradation of CR

TOC of initial CR solution (mg L^{-1})	TOC of CR solution after 80 min degradation (mg L^{-1})	TOC removal efficiency (%)
11.07	5.40	51.22

Table S11. Adsorption efficiency, photodegradation efficiency, first-order kinetic parameters for different samples (initial CR concentration: 100 mg L^{-1}, CR solution: 50 mL, pH: 6, and catalyst dosage: 25 mg).

Samples	Adsorption efficiency (%)	Adsorption+ Photodegradation efficiency (%)	k (min^{-1})	R^2
$Bi_{0.8}Y_{0.2}OBr$	14.28	62.24	0.01011	0.9997
$Bi_{0.8}Y_{0.2}OBr_{0.99}I_{0.01}$	15.45	54.28	0.0077	0.99973
$Bi_{0.8}Y_{0.2}OBr_{0.98}I_{0.02}$	26.97	84.38	0.01978	0.99752
$Bi_{0.8}Y_{0.2}OBr_{0.97}I_{0.03}$	37.07	92.62	0.0278	0.99472
$Bi_{0.8}Y_{0.2}OBr_{0.96}I_{0.04}$	38.72	91.41	0.02582	0.99591
$Bi_{0.8}Y_{0.2}OBr_{0.95}I_{0.05}$	35.07	88.38	0.02237	0.99415
$Bi_{0.8}Y_{0.2}OBr_{0.9}I_{0.1}$	49.31	92.07	0.02494	0.9752